JBC RESEARCH ARTICLE

Zafirlukast inhibits the growth of lung adenocarcinoma *via* inhibiting TMEM16A channel activity

Received for publication, November 18, 2021, and in revised form, February 8, 2022 Published, Papers in Press, February 15, 2022,
https://doi.org/10.1016/j.jbc.2022.101731

Sai Shi[1,2,3,‡], Biao Ma[1,2,3,‡], Fude Sun[3], Chang Qu[1,2,3], Gen Li[1,2,3], Donghong Shi[1,2,3], Wenxin Liu[4], Hailin Zhang[5], and Hailong An[1,2,3,*]

From the [1]State Key Laboratory of Reliability and Intelligence of Electrical Equipment, [2]Key Laboratory of Electromagnetic Field and Electrical Apparatus Reliability of Hebei Province, and [3]Key Laboratory of Molecular Biophysics, Hebei Province, Institute of Biophysics, School of Science, Hebei University of Technology, Tianjin, China; [4]Department of Gynecologic Oncology, Tianjin Medical University Cancer Institute and Hospital, Tianjin, China; [5]Department of Pharmacology, Hebei Medical University, Shijiazhuang, China

Edited by Mike Shipston

Lung cancer has the highest mortality among cancers worldwide due to its high incidence and lack of the effective cures. We have previously demonstrated that the membrane ion channel TMEM16A is a potential drug target for the treatment of lung adenocarcinoma and have identified a pocket of inhibitor binding that provides the basis for screening promising new inhibitors. However, conventional drug discovery strategies are lengthy and costly, and the unpredictable side effects lead to a high failure rate in drug development. Therefore, finding new therapeutic directions for already marketed drugs may be a feasible strategy to obtain safe and effective therapeutic drugs. Here, we screened a library of over 1400 Food and Drug Administration–approved drugs through virtual screening and activity testing. We identified a drug candidate, Zafirlukast (ZAF), clinically approved for the treatment of asthma, that could inhibit the TMEM16A channel in a concentration-dependent manner. Molecular dynamics simulations and site-directed mutagenesis experiments showed that ZAF can bind to S387/N533/R535 in the nonselective inhibitor binding pocket, thereby blocking the channel pore. Furthermore, we demonstrate ZAF can target TMEM16A channel to inhibit the proliferation and migration of lung adenocarcinoma LA795 cells. *In vivo* experiments showed that ZAF can significantly inhibit lung adenocarcinoma tumor growth in mice. Taken together, we identified ZAF as a novel TMEM16A channel inhibitor with excellent anticancer activity, and as such, it represents a promising candidate for future preclinical and clinical studies.

Cancer is the second leading cause of death worldwide after cardiovascular disease, accounting for approximately 10 million deaths each year or one-sixth of all annual deaths worldwide (1). According to a report provided by the World Health Organization in 2020, the number of incidences of lung cancer is 2.21 million, and the number of deaths is 1.79 million (2). Lung cancer is the highest mortality cancer. Significantly, Asia accounts for 59.6% and 61.9% of the global incidence and mortality rates of lung cancer, respectively, which is more than the rest of the world combined (3). Therefore, the development of antilung cancer drugs is particularly urgent, in addition to preventive measures such as promoting a healthy diet and avoiding tobacco use. Recently, many studies have shown that TMEM16A channels are upregulated in several human lung cancer cell lines and that overexpression of TMEM16A contributes to tumor growth and invasion in lung cancer (4). Further studies have shown that the TMEM16A gene is localized at 11q13, one of the most frequently amplified regions in human cancers and is associated with poor prognosis (5). Furthermore, knockdown and direct inhibition of TMEM16A channels can reduce the ability of lung cancer cells to proliferate, migrate, etc. (6). Several TMEM16A channel inhibitors, such as luteolin, matrine, etc., have been identified and have shown therapeutic effects on lung cancer (7, 8). Therefore, TMEM16A channels are promising as antilung cancer drug targets.

TMEM16A (also known as ANO1) is a Ca^{2+}-activated chloride channel. TMEM16A is mainly expressed in epithelial cells, smooth muscle cells, neuronal cells, and some cancer cells, and its main physiological functions are to regulate fluid secretion, smooth muscle contraction, and neuronal excitation (9–11). Dysfunction of TMEM16A channels has been associated with a variety of diseases, including cancer (12–15), hypertension (16), and asthma (17). Therefore, TMEM16A channel modulators have the potential to treat these diseases. In previous studies, to confirm the druggability of TMEM16A channels, we identified a TMEM16A channel inhibitor binding pocket, which is located in the extracellular vestibule, and the drug can bind to this pocket to block the ion-conducting pores (18). In addition, we found a natural product inhibitor of the TMEM16A channel, theaflavin, which was able to targets the TMEM16A channel to inhibit the viability of lung adenocarcinoma cells (19). Unfortunately, theaflavin is a polyphenolic compound with poor molecular stability, and further improvements are needed if it is to be used as an anticancer drug. Indeed, the development of anticancer drugs involves lead compound discovery, preclinical and clinical studies that

‡ These authors contributed equally to this work.
* For correspondence: Hailong An, hailong_an@hebut.edu.cn.

require clarification of their pharmacological properties, antineoplastic effects, and toxicity (20). The time from initial experiments to regulatory review is often over 10 years, with development costs ranging in the billions of dollars for per drug. Although there are tens of thousands of anticancer drugs in the research phase, the approval rate for anticancer drugs entering clinical research is less than 5% (21). Therefore, the development of new anticancer drugs is a high investment, long lead time, and high-risk task.

In this study, we propose a drug repurposing strategy using TMEM16A as an antilung cancer drug target. We identified an inhibitor drug targeting the TMEM16A channel by screening the Food and Drug Administration (FDA)-approved drug dataset based on the TMEM16A channel inhibitor binding pocket identified in previous studies. We revealed the molecular mechanism by which this drug inhibits the TMEM16A channel and tested its antilung cancer activity by inhibiting the TMEM16A channel in cells as well as in mice. The strength of this study is that the pharmacokinetics and toxicology of the novel antilung cancer drug discovered are known and its safety profile has been approved by the FDA, thus greatly increasing the likelihood of the drug passing the experimental phase. Although the dose safety and human efficacy of the discovered TMEM16A channel inhibitor will need to be tested in clinical studies, it is expected that the evaluation process will be significantly shortened based on the available data. Our strategy offers new ideas for the discovery of safe and effective anticancer drugs.

Results

Screening based on the inhibitor binding pocket revealed that ZAF is a TMEM16A inhibitor

In a previous study, we identified the extracellular vestibule of the TMEM16A channel as a nonselective inhibitor binding pocket and succeeded in discovering a potent channel inhibitor, theaflavin (19). However, theaflavins are susceptible to oxidation, resulting in unsatisfactory anticancer efficacy at the cellular level. To shorten drug development time and increase the success rate of drug trials, this study wanted to obtain inhibitors targeting the TMEM16A channel from marketed drugs, as these compounds were safety tested and had better pharmacokinetic properties. To achieve this goal, we screened a database of over 1400 FDA-approved drugs using the open-source molecular docking program Vina. We performed docking using the previously identified TMEM16A channel inhibitor binding pocket as the receptor docking region. The lower the binding energy of the small molecule to the protein indicates a higher affinity for both. We tested the four highest-ranked drugs based on drug–protein affinity using patch clamp (Fig. 1, *A* and *B*), which were: Conivaptan, Entrectinib, Pimaricin, and Zafirlukast.

First, patch clamp experiments showed that human embryonic kidney 293T cells (HEK293T) cells had no recordable currents, and HEK293T cells transfected with TMEM16A plasmid have recordable currents in the presence of 600 nM Ca^{2+}, and this current could be almost completely inhibited by 10 μM $T16A_{inh}$-A01 (TMEM16A specific inhibitor), indicating that the recorded current comes from TMEM16A channels (Fig. 1, *C* and *D*). Then, patch clamp testing of the four drugs showed that Zafirlukast (ZAF) at 100 μM concentration inhibited 90% of the TMEM16A current (Fig. 1*E*). The current–voltage analysis showed that the outward rectification current–voltage relationship characteristic of the TMEM16A channel was more obvious at low ZAF concentrations (Fig. 1, *F* and *G*). The concentration–response curve was fitted using the Hill function, revealing that the concentration giving half-maximal inhibition (IC_{50}) of ZAF for the inhibition of TMEM16A-mediated currents was 8.1 ± 1.2 μM (Fig. 1*H*). ZAF is an oral drug for the prevention and treatment of bronchial asthma. Its mechanism of action is to reduce asthma attacks by antagonizing cysteine leukotriene receptors thereby reducing airway smooth muscle contraction and inflammation. ZAF has been shown to be well tolerated in the treatment of asthma and can be taken orally for long periods with low toxicity. Here, we found that ZAF is an inhibitor of TMEM16 A channels and has the potential to treat TMEM16A-related diseases.

ZAF uses a vertical binding mode to block the pore

To reveal the molecular mechanism of inhibition of TMEM16A channels by ZAF, we constructed a complex simulation system, including TMEM16A, ZAF, and 1-palmitoyl-2-oleoyl-sn-glycero-3-phosphocholine (Fig. 2). Molecular docking revealed two different binding poses for ZAF at the highest affinity values: binding mode 1 (horizontal pose) and binding mode 2 (vertical pose) (Fig. 2). The A and B chains of the TMEM16A channel are two homologous subunits, and placing the two conformations of ZAF in the A and B chains of TMEM16A protein respectively enables monitoring the stability of the two binding modes in the same system. Three independent 200 ns all-atom simulations were performed for the complex simulation system. To evaluate the conformational stability of the complex system during Molecular dynamics (MD) simulations, we calculated the root mean square deviation (RMSD) of the TMEM16A and ZAF. As shown in Figure 3, *A*–*C*, RMSD values of the protein backbone atoms ranged between 2.52 and 2.80 Å, relative to the initial structure. The RMSD values for the ZAF heavy atoms in binding modes 1 and 2 were 1.95 to 3.01 Å and 0.88 to 1.45 Å, respectively, and the RMSD for binding mode 1 fluctuated dramatically, indicating that it was not stable in this binding mode. We extracted the conformations of the final and found that the conformations of the three trajectories of ZAF in binding mode 1 were significantly different, indicating that ZAF was unable to bind stably in binding mode 1 (Fig. 3, *D* and *E*). During the three dynamics, binding mode 2 maintained a similar binding pose to the initial state, and the RMSD of the ZAF molecule was smoother (Fig. 3*F*). This suggests that ZAF may use a vertical binding mode to bind TMEM16A protein.

To reveal the interaction mode of ZAF with the TMEM16A channel, we mapped the free energy landscape of ZAF bound to TMEM16A in binding mode 2. First, dynamics simulations showed that the benzene ring at the head of ZAF has a stable carbocyclic stacking relationship with residue W389 and that the nitrogen-containing heterocycle of ZAF is slightly

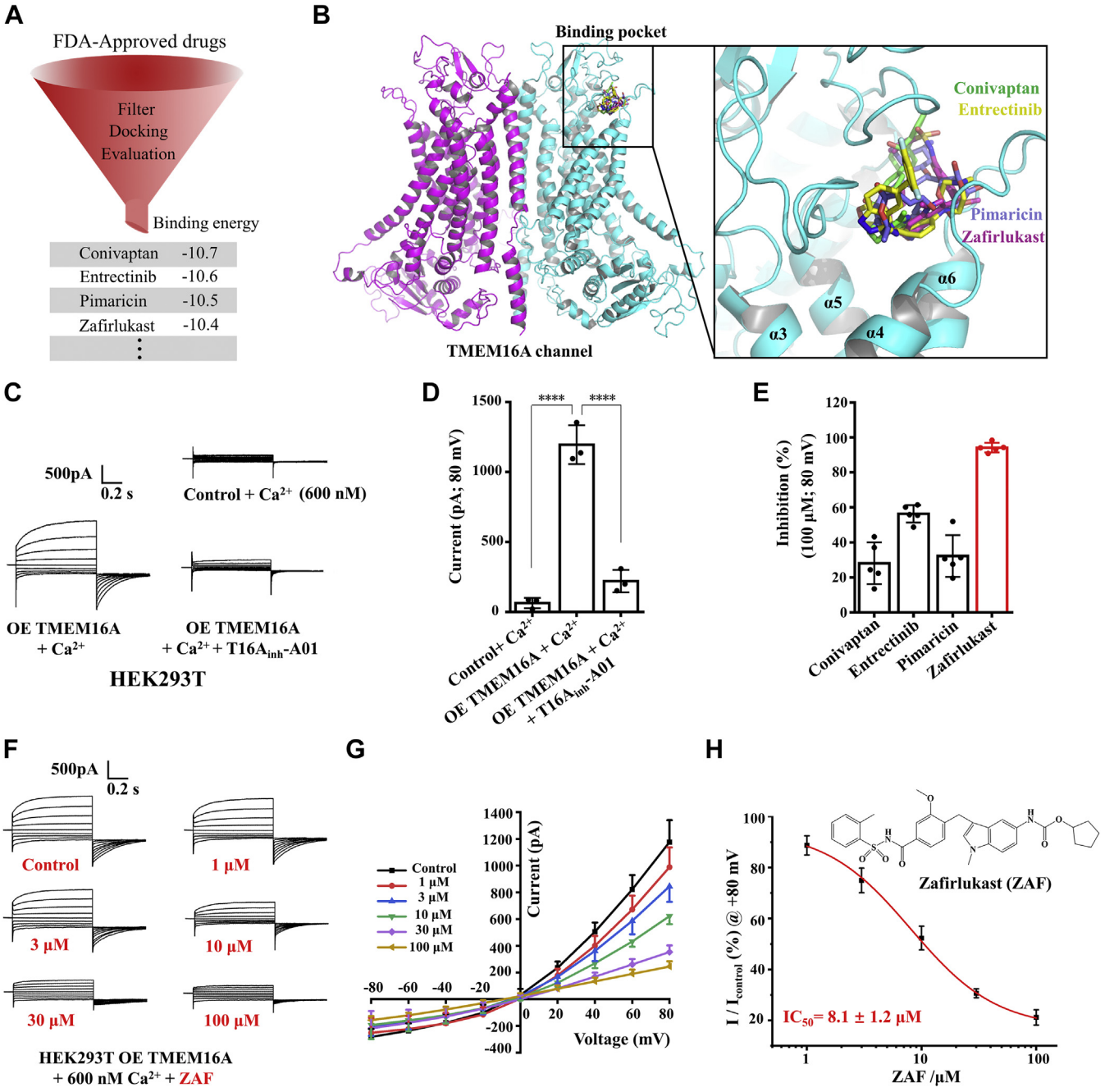

Figure 1. ZAF is a novel inhibitor of TMEM16A channel. *A*, virtual screening flowchart. *B*, TMEM16A channel inhibitor binding pocket. *C*, whole-cell currents of HEK293T cells overexpressing (OE) TMEM16A channels were activated by 600 nM Ca^{2+} in the pipette solution and inhibited by 10 μM of $T16A_{inh}$-A01. WT HEK293T as vehicle control. The stimulation protocol: a holding potential of 0 mV for 100 ms, the membrane voltage was clamped in steps of 20 mV from −80 to +80 mV for 750 ms, then back down to −80 mV for 500 ms. *D*, statistical results of the TMEM16A whole-cell current in (*C*). Data are means ± SD (n = 3; ****$p < 0.0001$, OE TMEM16A + Ca^{2+} *versus* control; ****$p < 0.0001$, OE TMEM16A + Ca^{2+} + $T16A_{inh}$-A01 *versus* OE TMEM16A + Ca^{2+}). *E*, the inhibition by Conivaptan, Entrectinib, Pimaricin, and Zafirlukast (100 μM) of TMEM16A current tested at +80 mV. Data are means ± SD (n = 5). *F*, representative current of TMEM16A inhibited by various concentrations of ZAF (0, 0.01, 0.1, 1, 10, and 100 μM). The stimulation protocol is consistent with (*C*). *G*, I-V curve of the TMEM16A currents inhibited with different concentrations of ZAF (n = 5). *H*, concentration response curves of ZAF inhibition of TMEM16A currents in HEK293T cells. The plot was fitted to the Hill equation (n = 5). HEK293T, human embryonic kidney 293T cells; I-V, current–voltage; ZAF, Zafirlukast.

redirected. We then calculated the distance between the benzene ring of the ZAF head and residue W389 and the overall folding angle of the molecule of ZAF and used these as reaction coordinates to plot the free energy landscape of protein–ligand binding. The data show the presence of a stable bound state of ZAF in binding mode 2 (Fig. 3*G*). As shown in Figure 3*H*, ZAF formed six interactions with the 22 residues in the binding pocket. Among them, H-bond interactions with S387, N533, and R535; π-π stacking interactions with W389, carbon-H-bond with M524, A523; alkyl interactions with A521, L522; and π-Sigma interactions with V538; and van der Waals interactions with P380, P627, L827, D825, L385, C386,

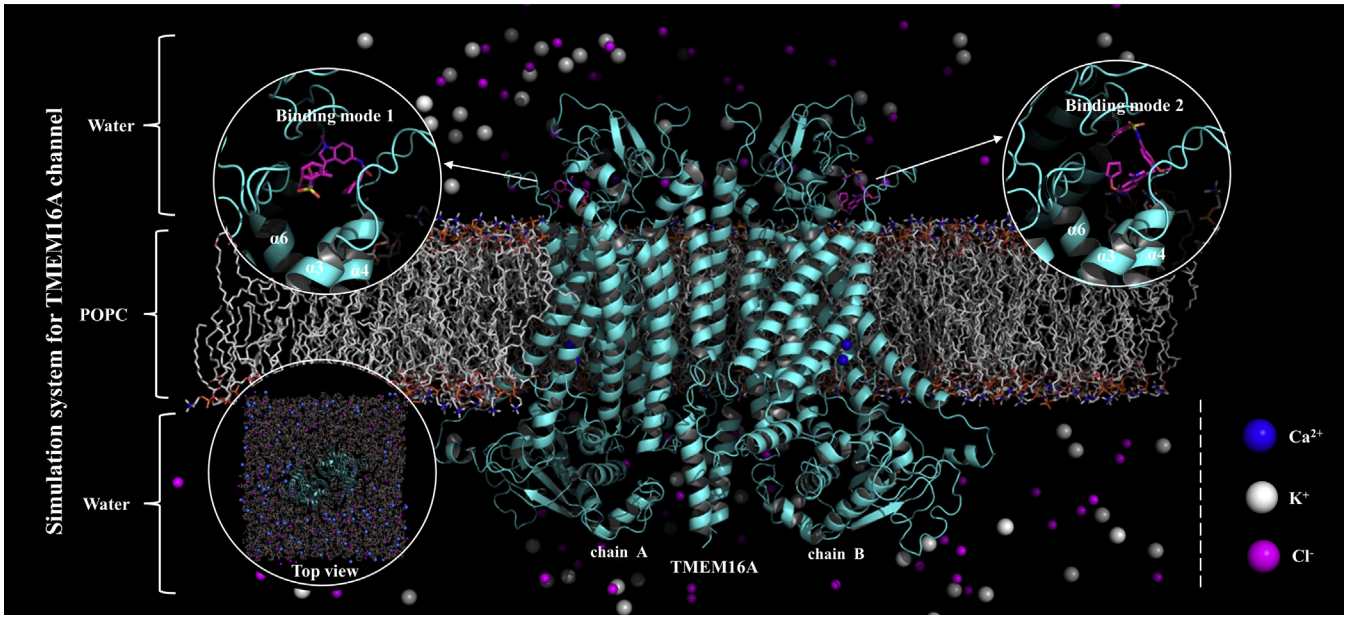

Figure 2. Molecular dynamics simulation of the TMEM16A system. TMEM16A is shown in *cartoon*; POPC is shown in *stick* (*gray*). ZAF is shown as *magenta sticks*. Two binding poses of ZAF were placed in the A and B chains of TMEM16A protein respectively. Ca^{2+}, K^+, and Cl^- ions are shown as *blue*, *white*, and *magenta spheres*, respectively. POPC, 1-Palmitoyl-2-oleoyl-sn-glycero-3-phosphocholine; ZAF, Zafirlukast.

C382 E624, A626, T539, S527, P528, and N525. These interactions allow the ZAF to bind stably above the pores of the TMEM16A channel and thus block the pore.

The sulfanilamide and amide groups are the key pharmacodynamic groups of ZAF

To reveal the molecular basis for the inhibition of TMEM16A channels by ZAF, we analyzed the binding mode of ZAF to TMEM16A channels. As shown in Figure 4, *A* and *B*, the sulfonamide and amide groups of ZAF form H-bond interactions with the S387, N533, and R535 side chains. We calculated the H-bond occupancy to assess the stability of these H-bonds, and as shown in Figure 4*C*, the occupancy of all five hydrogen bonds was higher than 30%. H-bond is an electrostatic interaction. To characterize the electrostatic interactions, we calculated the electrostatic surface potentials of ZAF with S387, N533, and R535 at the steadiest state. As shown in Figure 4, *D* and *E*, there is an overlap of van der Waals surfaces in the regions where all three residues form hydrogen bonds with ZAF, and the electrical properties of the overlapping regions are complementary. This suggests that the sulfanilamide and amide groups are the pharmacodynamic groups for ZAF inhibition of TMEM16A channels. To verify the binding mode of ZAF with the TMEM16A channel, we performed a molecular mutagenesis study. Patch clamp experiments showed that the TMEM16A triple mutant channel can be activated by 600 nM Ca^{2+} and inhibited by different concentrations of ZAF (Fig. 4*F*). The mutation does not change the outward rectification characteristics of the TMEM16A channel (Fig. 4*G*). The concentration–inhibition curve showed that the IC_{50} of ZAF inhibited TMEM16A mutant-mediated currents was 113.2 ± 2 μM, thus reducing the activity of ZAF inhibition of the TMEM16A mutant by approximately 14-fold compared to the WT (Fig. 4*H*). This suggests that the S387A/N533A/R535A mutation significantly weakened the inhibitory activity of ZAF inhibition of TMEM16A, and S387, N533, and R535 are key sites for TMEM16A inhibition by ZAF.

ZAF-targeted TMEM16A inhibits lung adenocarcinoma cell viability

To investigate whether ZAF has anticancer efficacy, we performed MTT and wound-healing assays. First, we tested the potency of different concentrations of ZAF in inhibiting the proliferation of lung adenocarcinoma cells LA795 which has endogenous high-expressing TMEM16A (Fig. 5, *A* and *B*). ZAF concentration-dependently inhibited the proliferation of LA795 cells, with 50, 75, and 100 μM ZAF reducing the proliferation capacity of LA795 cells by 27.3%, 55.5%, and 67.3%, respectively (Fig. 5*C*). Knockdown of the TMEM16A channel by shRNA significantly reduced LA795 cell proliferation, while the use of ZAF did not further inhibit the proliferation of LA795 cells with knockdown of TMEM16A expression (Fig. 5, *A*, *B*, and *D*). In addition, we examined the effect of ZAF on the proliferation of 16HBE (human bronchial epithelial) cells with very low expression of TMEM16A channel, and the data showed that 100 μM ZAF did not affect the proliferation of 16HBE (Fig. 5, *E*–*G*). However, when 16HBE cells were transfected with TMEM16A plasmid, ZAF exhibited a significant inhibitory effect on the proliferation of 16HBE cells with high expression of the TMEM16A channel. 100 μM ZAF reduced the proliferation capacity of 16HBE cells by 57.04% (Fig. 5, *E*, *F*, and *H*). We also tested the effect of TMEM16A expression on the proliferation of 16HBE cells. The data showed that the expression of TMEM16A WT and triple mutants contributed to the proliferation of 16HBE cells.

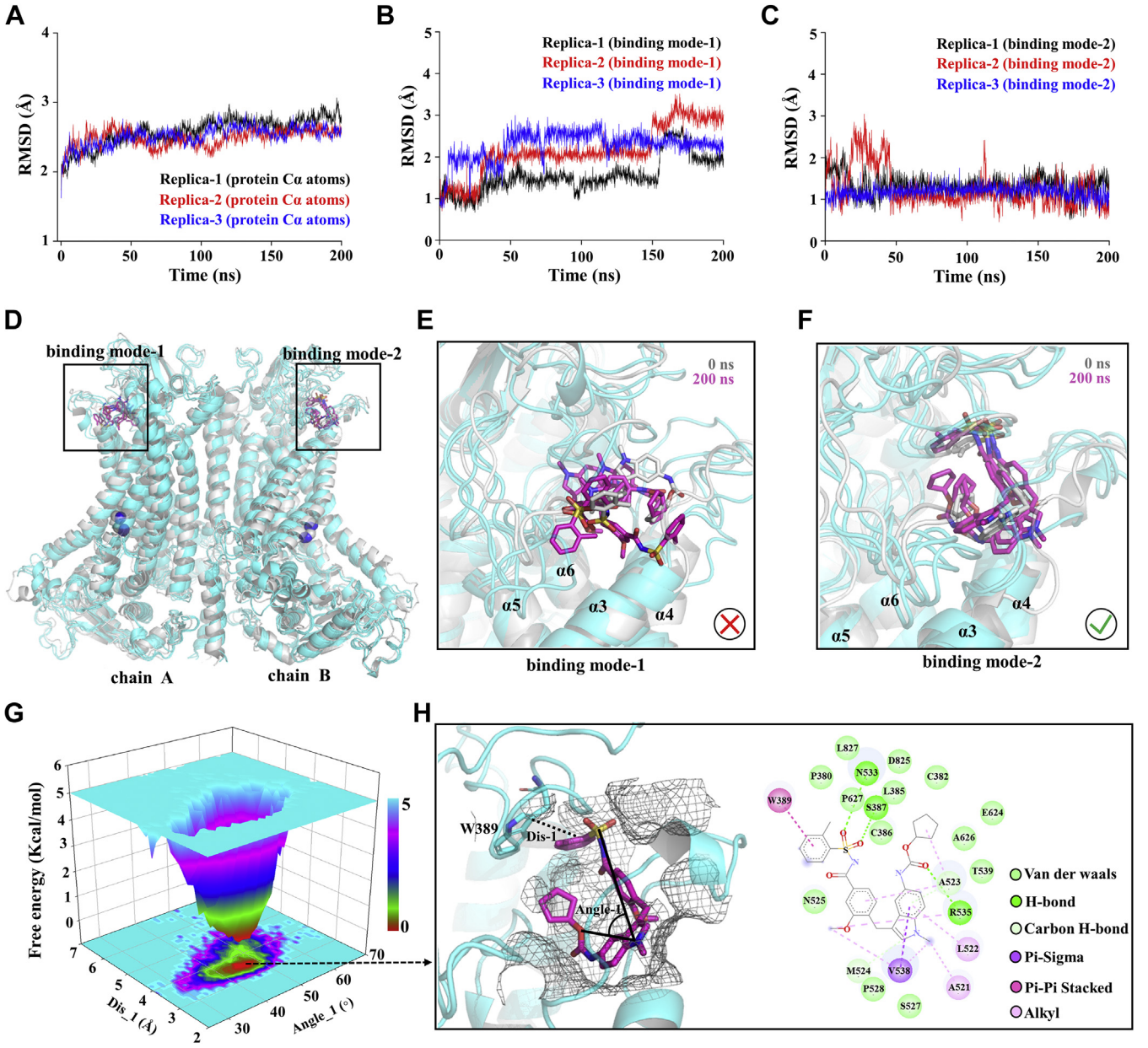

Figure 3. Binding mode of ZAF and TMEM16A. *A*, the RMSD of the protein. *B* and *C*, the RMSD of the ZAF heavy atoms. *D*, the final state of receptors and ligands of the system. *E* and *F*, the overlap of the final state (200 ns, three repetitions) and initial state (0 ns) structure of the two binding modes. *G*, free energy landscape of the ZAF binding mode. *H*, representations of the binding mode of the ZAF and TMEM16A in their lowest binding energy conformation. ZAF, Zafirlukast.

Importantly, 100 μM ZAF reduced the proliferation of 16HBE cells expressing TMEM16A WT and triple mutants by 38.2% and 17.9%, respectively (Fig. 5, *E*, *F*, and *I*). In addition, cell proliferation was not affected after transfection of 16HBE cells with an empty vector (Fig. 5*I*). The above experiments showed that ZAF could inhibit the proliferation of lung cancer cells by inhibiting the TMEM16A channel.

The migration behavior of cancer cells is critical for tumor metastasis. A statistical result shows that TMEM16A promotes cell migration and invasion in various tumors such as head and neck squamous cell carcinoma, hepatocellular carcinoma, glioblastoma, gastric cancer, etc (22). We performed a wound-healing assay to evaluate the effect of ZAF on the migration of LA795 cells (lung adenocarcinoma cell line). Different concentrations of ZAF were added to the medium with LA795 cells, and the cells were observed for 72 h. As shown in Figure 5, *J* and *K*, only 12% of the wound area could be observed in the control group after 72 h. In the 25 μM, 50 μM, and 75 μM groups, 33%, 63%, and 88% of the total wound area were observed after 72 h, respectively. It should be noted that ZAF above 50 μM had a significant inhibitory effect on LA795 cell activity; therefore, the inhibition of cell migration by high concentrations of ZAF cannot be excluded as being due to cell death. However, 25 μM ZAF had almost no effect on LA795 cell viability but still significantly inhibited LA795 cell migration

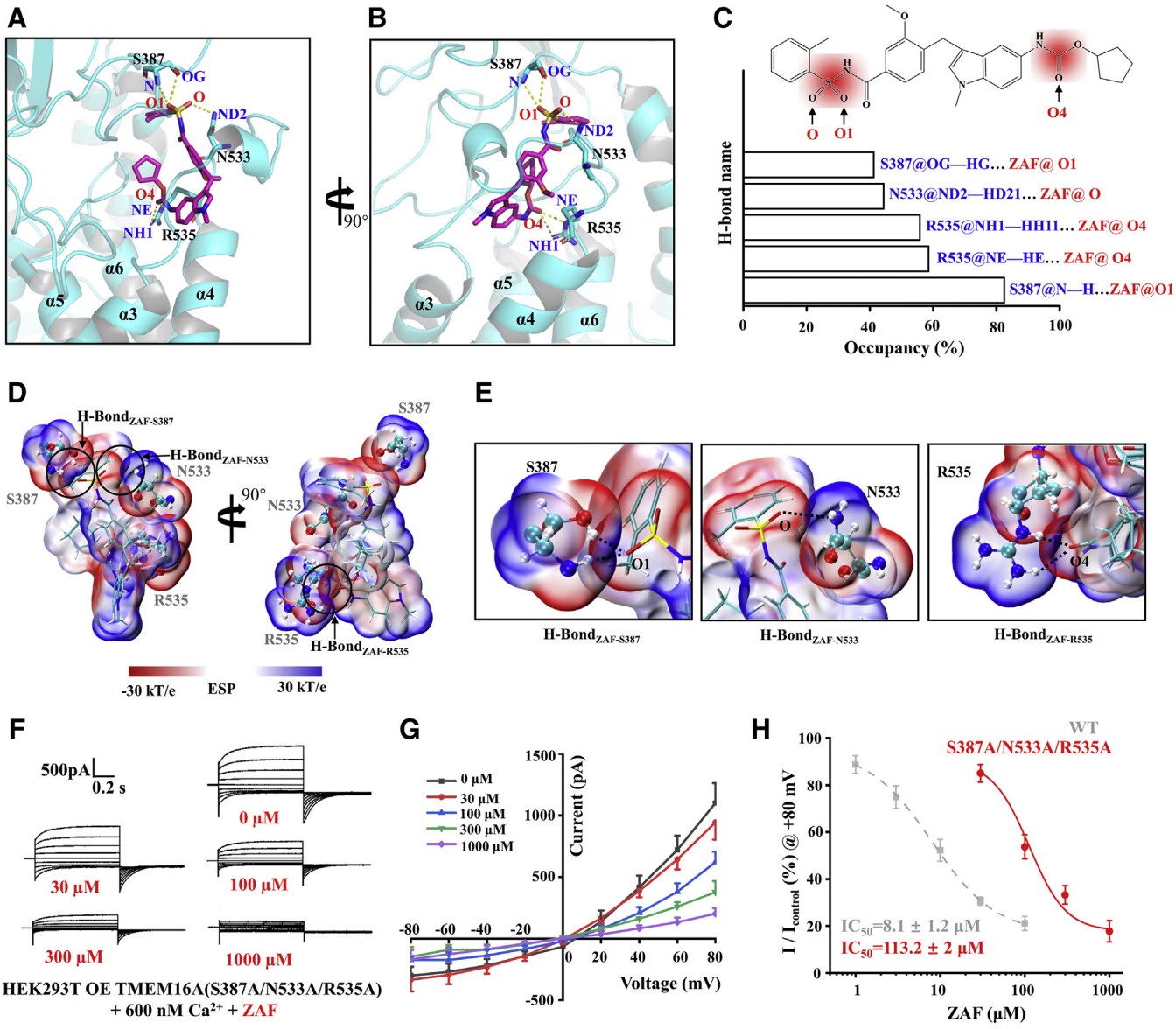

Figure 4. Identification of ZAF binding sites. *A* and *B*, binding mode of ZAF and TMEM16A protein. ZAF is shown as *magenta sticks*. Binding residues S387, N533, and R535 are shown as *cyan sticks*. *C*, H-bond occupancy between the ZAF and S387/N533/R535. The *red regions* in the molecular structure are the amide group and the sulfonamide group of ZAF. *D*, ESP-mapped molecular van der Waals surface of ZAF and S387/N533/R535. The *stick* represents ZAF. Sphere model represents residues. *E*, H-bond between ZAF and S387/N533/R535. *F*, representative current of TMEM16A mutant inhibited by various concentrations of ZAF (0, 30, 100, 300, 1000 μM). The stimulation protocol is consistent with Figure 1*C*. *G*, I-V curve of the TMEM16A mutant (S387A/N533A/R535A, HEK293T cells) currents inhibited with different concentrations of ZAF (n = 5). *H*, concentration response curves for ZAF inhibition of TMEM16A mutants, and for comparison, *dashed lines* are used to show the concentration response curves of ZAF for WT TMEM16A (data from Fig. 1*G*). The plot was fitted to the Hill equation (n = 5). ESP, electrostatic surface potential; I-V, current–voltage; ZAF, Zafirlukast.

(Fig. 5, *C*, *J*, and *K*). Therefore, the inhibitory effect of ZAF on cell migration at low concentrations is clear.

Besides, the anticancer efficacy of ZAF was also evaluated in a visualized manner by live/dead staining, where live and dead cells were differentiated by co-staining with Calcein AM (green fluorescence; living cells) and propidium iodide (red fluorescence; dead cells). As presented in Figure 5*L*, in the control group, all of the cells exhibited green fluorescence. Meanwhile, LA795 cells incubated with 50 and 100 μM ZAF were killed to varying degrees and stained with red fluorescence. Taken together, this evidence suggests that ZAF has excellent anticancer activity *in vitro*.

ZAF inhibited the growth of lung adenocarcinoma in vivo

To test the inhibitory effect of ZAF on tumors growth *in vivo*, a tumors transplantation model of the lung adenocarcinoma cell line LA795 was constructed. Figure 6*A* showed the time of data collection and dosing in the animal model test. The inhibition of tumors growth by ZAF was examined by measuring tumors volume. The data showed that tumors growth was significantly higher in the control group than in the experimental group using drugs. The tumors growth rate of the mice in the experimental group with low dose of ZAF (2.9 mg/kg) and the experimental group with cisplatin (6.5 mg/kg) was close, while the tumors growth rate was slowest in the

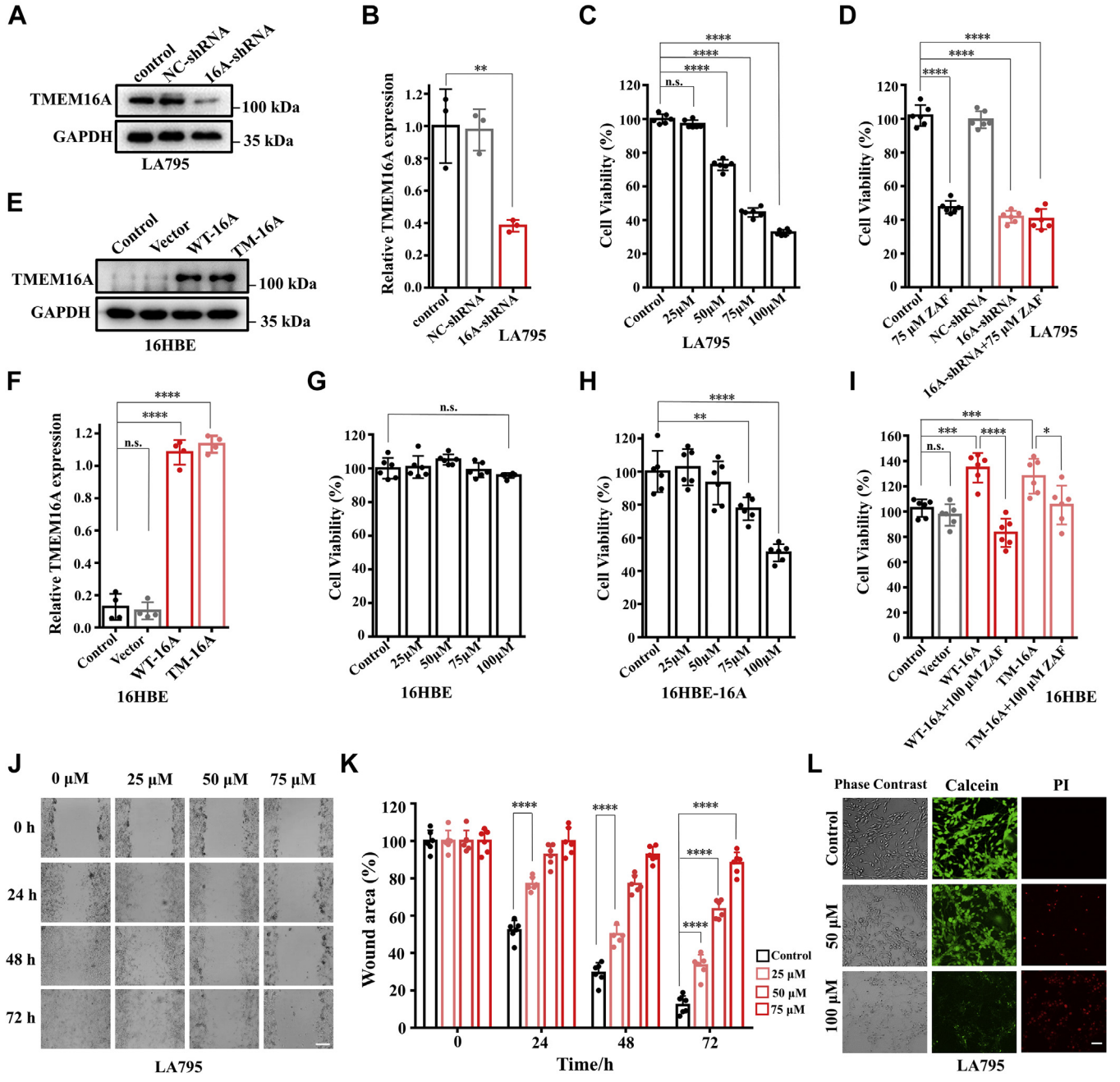

Figure 5. ZAF inhibited proliferation and migration of LA795 cells. *A*, Western blot images of TMEM16A expression in LA795 cells. The image is from one gel. *B*, the expression of TMEM16A was normalized to the expression level of GAPDH (HEK293T cells). Data are means ± SD. One-way ANOVA followed by Tukey HSD test (n = 3; $^{**}p = 0.009$, 16A-shRNA *versus* control). *C*, inhibitory effect of ZAF to the proliferation of LA795. Data are means ± SD. One-way ANOVA followed by Tukey HSD test (n = 6; n.s. $p = 0.075$, 25 μM ZAF *versus* control; $^{****}p < 0.0001$, 50 μM ZAF *versus* control; $^{****}p < 0.0001$, 75 μM ZAF *versus* control; $^{****}p < 0.0001$, 100 μM ZAF *versus* control). *D*, statistics results of cell viability after transfection with shRNA-16A. Data are means ± SD. One-way ANOVA followed by Tukey HSD test (n = 6; $^{****}p < 0.0001$, 75 μM ZAF *versus* control; $^{****}p < 0.0001$, 16A-shRNA *versus* control; $^{****}p < 0.0001$, 16A-shRNA+75 μM ZAF *versus* control). *E*, Western blot images of TMEM16A expression in 16HBE cells. The image is from one gel. *F*, the expression of TMEM16A was normalized to the expression level of GAPDH (16HBE cells). Data are means ± SD. One-way ANOVA followed by Tukey HSD test (n = 4; $p = 0.642$, vector *versus* control; $p < 0.0001$, WT-16A [16HBE cells over expression wild type-TMEM16A] *versus* control; $p < 0.0001$, TW-16A [16HBE cells over expression triple mutant-TMEM16A(S387A/N533A/R535A)] *versus* control). *G*, inhibitory effect of ZAF to the proliferation of 16HBE. Data are means ± SD. One-way ANOVA followed by Tukey HSD test (n = 6; n.s. $p = 0.126$, 100 μM ZAF *versus* control). *H*, inhibitory effect of ZAF to the proliferation of 16HBE transfected with TMEM16A. Data are means ± SD. One-way ANOVA followed by Tukey HSD test (n = 6; $^{**}p = 0.003$, 75 μM ZAF *versus* control; $^{**}p < 0.0001$, 100 μM ZAF *versus* control). *I*, the effect of TMEM16A expression on the proliferation of 16HBE cells. Data are means ± SD. One-way ANOVA followed by Tukey HSD test (n = 6; n.s. $p = 0.251$, vector *versus* control; $^{***}p = 0.0018$, WT-16A *versus* control; $^{***}p = 0.0025$, TM-16A *versus* control; $^{****}p < 0.0001$, WT-16A *versus* WT-16A + 100 μM ZAF; $^{*}p = 0.022$, TM-16A *versus* TM-16A + 100 μM ZAF). *J*, migration of LA795 cells in the presence of 0, 25, 50, and 75 μM ZAF was assessed by wound healing assay. Scale bar: 100 μm. *K*, statistical results of wound area in (*F*). Data are means ± SD. One-way ANOVA followed by Tukey HSD test (n = 6; $^{****}p < 0.0001$, 25 μM ZAF 24 h *versus* control 24 h; $^{****}p < 0.0001$, 50 μM ZAF 48 h *versus* control 48 h; $^{****}p < 0.0001$, 75 μM ZAF 72 h *versus* control 72 h; $^{****}p < 0.0001$, 75 μM ZAF 72 h *versus* 25 μM ZAF 72 h; $^{****}p < 0.0001$, 75 μM ZAF 72 h *versus* 50 μM ZAF 72 h). *L*, live-dead staining images of LA795 cells. Scale bar: 500 μm (n = 6). 16HBE, human bronchial epithelial cells; HSD, honestly significant difference; ZAF, Zafirlukast.

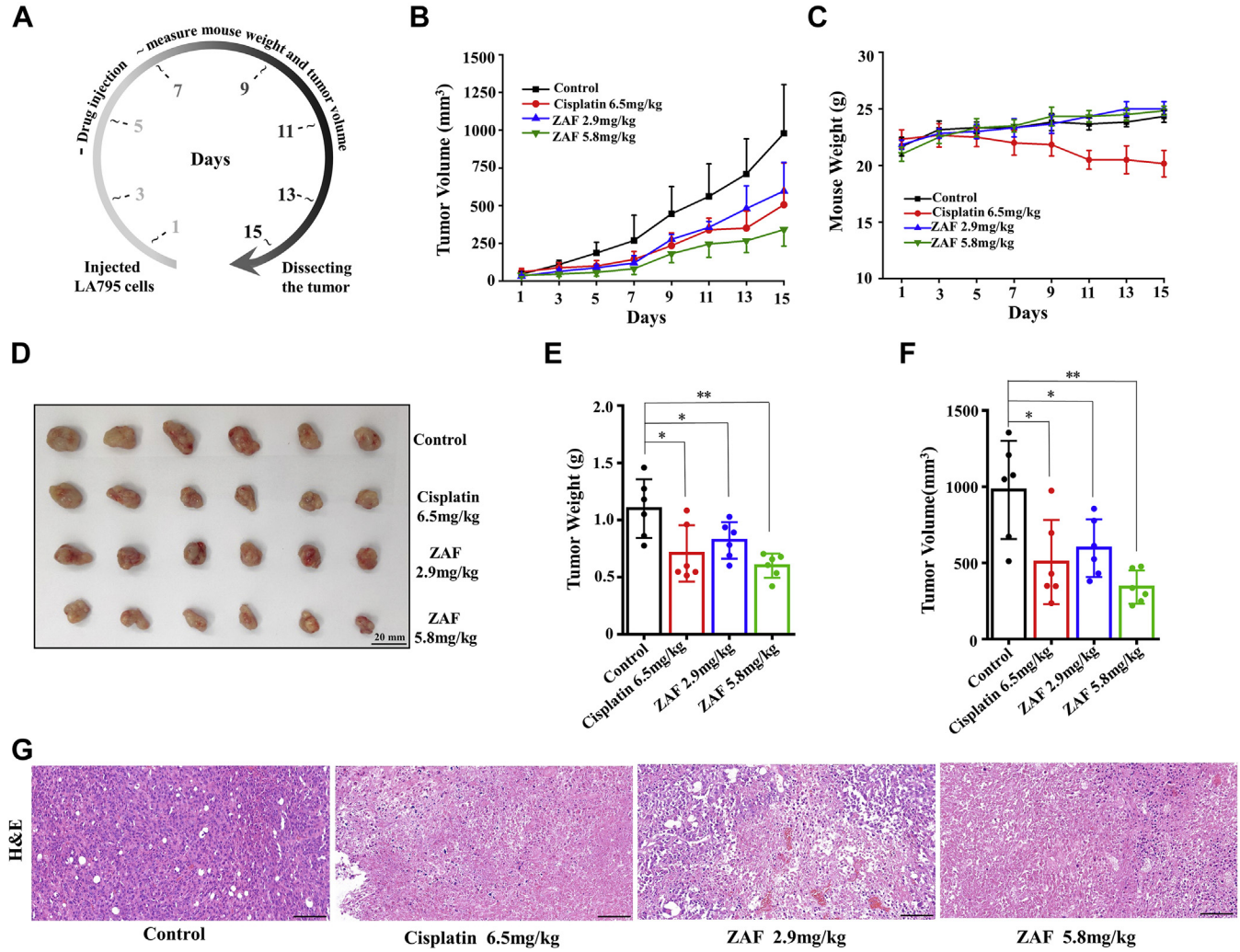

Figure 6. ZAF inhibits the growth of tumors *in vivo*. *A*, schematic diagram of experimental design and treatment. *B*, tumor volume growth curve in different groups (n = 6). *C*, body weight growth curve in different groups (n = 6). *D*, stripped images of the tumor entity after 7 administrations (n = 6). *E*, statistical results of the stripped tumor weight in (*D*) (n = 6). Data are means ± SD. One-way ANOVA followed by Tukey HSD test (n = 6; **p* = 0.022, Cisplatin 6.5 mg/kg *versus* control; **p* = 0.047, ZAF 2.9 mg/kg *versus* control; ***p* = 0.0013, ZAF 5.8 mg/kg *versus* control). *F*, statistical results of the stripped tumor volume in (*D*). Data are means ± SD. One-way ANOVA followed by Tukey HSD test (n = 6; **p* = 0.021, Cisplatin 6.5 mg/kg *versus* control; **p* = 0.031, ZAF 2.9 mg/kg *versus* control; ***p* = 0.001, ZAF 5.8 mg/kg *versus* control). *G*, histological sections of an excised tumor of each group after treatment. 20×. Scale bar: 50 μm. HSD, honestly significant difference; ZAF, Zafirlukast.

experimental group with high dose of ZAF (5.8 mg/kg) (Fig. 6*B*). The data also showed that there was a significant increase in the body weight of mice in the control and ZAF-administered experimental groups, while there was a significant decrease in the body weight of mice in the cisplatin-administered experimental group (Fig. 6*C*).

The inhibitory activity of ZAF on tumors growth was tested by dissecting the mice to examine the weight and volume of the tumors. As shown in Figure 6, *D–F*, the weight of tumors in each group of mice 15 days after tumors transplantation was 1.1 g (control), 0.7 g (Cisplatin 6.5 mg/kg), 0.82 g (ZAF 2.9 mg/kg), and 0.59 g (ZAF 5.8 mg/kg), and the volume was 978.9 mm^3 (control), 505.9 mm^3 (Cisplatin 6.5 mg/kg), 597.2 mm^3 (ZAF 2.9 mg/kg), and 341.3 mm^3 (ZAF 5.8 mg/kg). The above data indicated that ZAF had a significant inhibitory effect on lung adenocarcinoma tumors growth in tumor-transplanted mice. In addition, ZAF had no significant effect on the body weight of the mice, whereas cisplatin inhibited lung adenocarcinoma tumors growth in the tumor-bearing mice to a certain extent, but the body weight of the mice in the cisplatin experimental group was significantly lower, suggesting that ZAF may be safer. Finally, the antitumor efficacy of ZAF was further investigated by the hematoxylin and eosin staining assay. As shown in Figure 6*G*, the control group presented compact tumor cells in violet, whereas severe necrosis and pathological changes were exhibited in the tumor tissues treated with cisplatin and high concentrations of ZAF, which confirmed the excellent therapeutic effect of ZAF.

Discussion

Lung cancer is characterized by high incidence and mortality, and the discovery of antilung cancer drugs is urgent, but the development of an effective anticancer drug is challenging (23). Considering TMEM16A is a potential drug target for

lung cancer, to shorten the drug development time and improve the success of drug development, we screened a TMEM16A channel inhibitor drug, ZAF, from the FDA-approved drug library. We used molecular dynamics simulations, quantum chemistry calculations, and molecular biology experiments to confirm TMEM16A is a new target for ZAF. The results of calculations and site-directed mutations show that ZAF can bind residues R535, N533, and S387 above the pore, thereby blocking the pore. MTT and wound healing assays showed that ZAF could inhibit the proliferation and migration of lung cancer cells by inhibiting TMEM16A. In tumor-xenograft mouse experiments, ZAF showed significant inhibition of lung cancer tumor growth. The discovery of ZAF is a successful application of a novel screening strategy based on TMEM16A channel inhibitors binding pocket. On the one hand, this study identifies a new target of ZAF, the TMEM16A channel; on the other hand, the inhibition of TMEM16 by ZAF gives it potential as a novel antilung cancer drug.

Drug repurposing has become one of the most active areas in recent years, as this approach can significantly reduce the cost and time of inventing new drugs (24). Another reason for the low efficiency of conventional drug development is the lack of systematic evaluation of indications, which can therefore lead to unintended side effects (25). Successful examples of drug repurposing include sildenafil, Avastin, Minoxidil, etc (26). ZAF started as a cysteinyl leukotriene receptor antagonist. Cysteinyl leukotrienes (Cys-LTs, three major Cys-LT: LTC4, LTD4, and LTE4) are potent proinflammatory mediators produced by arachidonic acid in response to the action of 5-oxidoreductase. By competitively binding to Cys-LTs receptors (Cys-LT1R and Cys-LT1R: two distinct G-protein-coupled receptors), ZAF can block the action of Cys-LTs and relieve the symptoms of many chronic diseases, particularly bronchial asthma (27). ZAF displaced LTD4 with an IC_{50} value of 45.4 nM on the Cys-LT1R but was found to be inactive on the Cys-LT2R (28). Clinical trials have shown that patients with asthma produce the most consistent response when taking 20 mg of ZAF orally twice a day, with a 27% reduction in asthma symptoms (29). In an animal model for the treatment of asthma, guinea pigs administered ZAF orally at a dose of 0.5 μmol/kg(≈0.287 mg/kg) were able to achieve maximum antagonistic activity against LTD4 (30). Herein, the maximum dose administered in the xenograft tumor assay in mice was 5.8 mg/kg, which is approximately 20 times the dose administered in the guinea pig asthma model. Therefore, the potential side effects of ZAF need to be taken care of when using ZAF to treat lung cancer.

Recent studies have shown that ZAF can also prevent cardiovascular disease by inhibiting soluble epoxide hydrolase and inhibiting peroxisome activated receptors (31). A study in 2020 showed that ZAF is a thiol isomerase inhibitor that can concentration-dependently reduce platelet aggregation and granule secretion and that ZAF reduces thrombosis *in vivo* without impairing or increasing bleeding in a mouse test, so ZAF may be developed as a therapeutic agent for thrombosis (32). Notably, ZAF has been reported to block another chloride channel, the volume-regulated anion channel, with an IC_{50} = ∼17 μM. Studies have shown that volume-regulated anion channel may serve as a therapeutic target for stroke, and thus ZAF may have some therapeutic effect on stroke (33). These studies suggest that ZAF has a clear pharmacological mechanism and diverse therapeutic effects.

We found that ZAF could concentration-dependently inhibit TMEM16A channel currents and that mutations in key residues caused reduced sensitivity of ZAF to TMEM16A channels, thus confirming that ZAF can act as a TMEM16A channel inhibitor. Electrostatic interaction analysis showed that sulfonamide and amide groups are the key sites for ZAF to bind TMEM16A (Fig. 4). Notably, a 2019 study showed that ZAF inhibits receptor activity by binding to the pocket between cysteinyl leukotriene receptor TM4/TM5/TM7. Similarly, the sulfonamide and amide groups of ZAF can have a wide range of polar interactions with residues in the ligand pocket of the cysteinyl leukotriene receptor (34). Therefore, these two groups may constitute the key pharmacodynamic groups of ZAF. Crucially, we found that ZAF could inhibit the proliferation and migration of lung adenocarcinoma LA795 cells by inhibiting the activity of TMEM16 A channels. Further studies showed that ZAF had a significant inhibitory effect on tumors in lung adenocarcinoma–transplanted mice and did not affect the body weight of the mice. This suggests that ZAF can inhibit the growth of lung adenocarcinoma cells by targeting the TMEM16A channel. This is a preliminary indication that ZAF is a promising and safe antilung adenocarcinoma drug.

Although our group has previously identified numerous small molecules that have inhibitory effects on lung adenocarcinoma, such as theaflavin (19), arctigenin (35), and silibinin (36), the pharmacology and toxicology of these natural products are unknown, and these compounds require long-term testing and optimized modifications before they can hope to pass the evaluation phase. Based on pharmacokinetic studies and clinical use of ZAF, the drug has shown a better safety and stability profile than many natural products. However, the use of ZAF as an antilung adenocarcinoma drug requires more intensive trials and a safety assessment. Considering the numerous clinical data accumulated during the use of ZAF in the treatment of asthma, the evaluation process for ZAF will be considerably shorter.

Interestingly, TMEM16A channels are highly expressed in airway smooth muscle cells as well as in the secretory cells of airway patients, and TMEM16A channel inhibitors themselves have therapeutic potential for asthma (17). Firstly, inhibition of TMEM16A channels reduces the secretion of mucin from airway secretory cells and relieves airway smooth muscle contraction, both of which are beneficial in the treatment of asthma (37). Thus, inhibition of TMEM16A channels by ZAF may also be a route to treating asthma. In addition, TMEM16A channel inhibitors have the potential to inhibit dorsal root ganglion neuronal excitability and attenuate cerebral artery constriction, so ZAF may have potential therapeutic effects on neuropathic pain and hypertension. In conclusion, our results suggest that a drug repurposing strategy based on the TMEM16A channel as an antilung adenocarcinoma target is a

promising and promising approach for drug screening. Furthermore, the discovery of ZAF will facilitate the research process of antilung cancer drugs and provide opportunities for the discovery of drugs for the treatment of diseases associated with the TMEM16A channel.

Experimental procedures

Drug screening

The calcium-bound structure of TMEM16A (PDB ID: 5OYB) (38) was used as a docked receptor, and the missing short loops were complemented using the SWISS-MODEL program (39, 40). Virtual screening of drugs was performed using the molecular docking program Vina (41). The database contains 1435 FDA-approved drug molecules. Autodock tool (42) was used to prepare the PDBQT files of TMEM16A and drugs. The receptor was programmed to remain rigid, while the ligand was flexible. The grid center was determined according to the center of the upper inhibitor binding pocket of the pore, with a searching space size of 24 $Å^3$. The global search exhaustiveness value was set to 50. The maximum energy difference between the optimal binding mode and the worst case was set to 5 kcal/mol to ensure diverse docked poses. Conivaptan and Zafirlukast were purchased from DeSiTe (Chengdu, China). Entrectinib, Pimaricin, and $T16A_{inh}$-A01 were purchased from TargetMol.

Molecular dynamics simulations

The TMEM16A simulation system was constructed using CHARMM-GUI (43). TMEM16A protein was inserted into the 1-palmitoyl-2-oleoyl-sn-glycero-3-phosphocholine lipid bilayers, and 150 mM KCl was added to the solvated system. The final simulation boxes contained approximately 350,000 atoms and dimensions of ~171 × 171 × 146 $Å^3$. All simulations were performed using Amber16 (44). The Amber ff14SB force field, the lipid14 force field, and the Joung/Cheatham ion parameters (45, 46) were used. Parametrization of ZAF was performed using the Antechamber module of Amber16, using the Generalized Amber Force Field to assign atom types and the AM1-BCC method to assign charges.

First, the simulated system of solutions, membranes, and the entire system were sequentially performed for energy minimization. Next, the system temperature was increased from 0 to 100 K under the NVT ensemble, and then, the temperature was increased from 100 to 300 K under the NPT ensemble, during which the protein was restraint (10 kcal mol^{-1} $Å^{-2}$). An NPT equilibration of 500 ps was then performed, during which the water molecules filled the pore, and protein C_α atoms were restrained, with a constraint force of 2 kcal mol^{-1} $Å^{-2}$. Finally, for the simulation system, three independent 200 ns simulations were performed under NPT conditions at 300 K and 1 bar.

During the production process, the system used a Langevin thermostat and a Monte Carlo constant pressure device; the system showed an anisotropic pressure coupling with a nonviscous cutoff of 10 Å. Long-range electrostatic interactions were described by the Particle Mesh Ewald algorithm with a cutoff of 12 Å. The van der Waals interactions were cutoff at 12 Å. The lengths of hydrogen-containing covalent bonds were constrained using SHAKE, and the MD time step was set to 2 fs. The snapshots were extracted every 100 ps for all equilibrium MD trajectories to calculate statistical distributions. The CPPTRAJ module of the Amber program was used to analyze the generated trajectories.

Quantum chemical calculation

Density functional theory was used to calculate electrostatic surface potential analysis of drugs and residues. Gaussian 03 (47) was used to calculate the molecular wave function information. Wave function data used in all analyses were generated using the B3LYP/6-31G** level algorithm. Molecular surface analysis maps were generated by Multiwfn (48) and VMD 1.9.2 program (49).

Cell culture and transfection

HEK293T, LA795, and 16HBE cells were cultured in Dulbecco's Modified Eagle's medium and RPMI-1640 at a humid atmosphere (37 °C with 5% CO_2) respectively. The culture medium was supplemented with 10% FBS and 1% penicillin–streptomycin. The HEK293T and 16HBE cells were transfected with cDNA for mouse TMEM16A (Accession Number NM_178642.5) using Neofect DNA transfection reagent (Neofect). Following transfection, the HEK293T cells were maintained in Dulbecco's Modified Eagle's medium at 37 °C for 24 h before patch recording. The shRNA plasmid was transfected into cells with the above transfection reagent to knockdown the expression of endogenous TMEM16A in LA795 cells. TMEM16A-shRNAs had the following target sequence: 5′-CCTGCTAAACAACATCATT-3′. NC-shRNA was an expression vector containing nonspecific shRNA: 5′-TTCTCCGAACGTGTCACGT-3′.

Site-directed mutagenesis

The site-directed mutagenesis primers were designed by Agilent Primer Design Website (https://www.agilent.com/store/primerDesignProgram.jsp). Fast Mutagenesis System Kit (FM111-02, Transgen) was used for the site-directed mutagenesis experiments with a 50 μl PCR system and confirmed by DNA sequencing. The primer design sequence is provided in the Table 1.

Electrophysiology

Whole-cell patch clamp experiments were performed using HEK293T cells at room temperature (22–25 °C). Drug effects were quantified by measuring the drug-induced changes in current amplitude at −80 or +80 mV. Current–voltage (I-V) relationships were determined using step pulses between −80 and +80 mV in increments of 20 mV from a holding potential of 0 mV followed by −80 mV step. The currents were recorded from different cells exposed to different ZAF concentrations. The concentration-inhibition curve of ZAF on TMEM16A currents at +80 mV was calculated as follows: $I/I_{control}$, where $I_{control}$ indicates currents before ZAF application, and I represents the steady-state current after application of ZAF (This normally takes about 5 min). The value of IC_{50} was calculated by fitting the Hill equation.

Table 1
The design sequence of the primer

Primer	Sequence (5′ to 3′)	Number of nucleobase
S387A	gagctcatcttccagtaggcgcaggtcttgtcacacag	38
S387Aa	ctgtgtgacaagacctgcgcctactggaagatgagctc	38
N533A	actgtaacccggatggcggaccgcacagacgg	32
N533Aa	ccgtctgtgcggtccgccatccgggttacagt	32
R535A	gccgtgactgtaaccgcgatgttggaccgcac	32
R535Aa	gtgcggtccaacatcgcggttacagtcacggc	32

The external solution contained: NaCl, 160 mM; KCl, 2.5 mM; $CaCl_2$, 2 mM; $MgCl_2{\cdot}6H_2O$, 1 mM; glucose, 8 mM; Hepes, 10 mM (adjusted to pH 7.4 with NaOH). The pipette solution contained: CsCl, 130 mM; EGTA, 10 mM; $MgCl_2{\cdot}6H_2O$, 1 mM; Hepes, 10 mM; ATP, 2 mM (adjusted to pH 7.3 with CsOH). The 600 nM free Ca^{2+} pipette solution was prepared by adding standard $CaCl_2$ solution. The free Ca^{2+} concentration was calculated with Ca-EGTA calculator V1.2 (https://somapp.ucdmc.ucdavis.edu/pharmacology/bers/maxchelator/CaEGTA-NIST.htm).

All recordings were performed using an EPC10 amplifier controlled by Pulse software with a Digi LIH1600 interface (HEKA). The data were low-pass filtered at 2.9 kHz and sampled at 10 kHz.

Western blot

Different groups of LA795 and 16HBE cells were washed three times in ice-cold phosphate buffer solution and lysed in RIPA buffer with 1 X Halt phosphatase and protease inhibitor cocktails. The proteins were separated on 10% sodium dodecyl sulfate-polyacrylamide gels and electroblotted onto a nitrocellulose membrane in 25 mM Tris and 190 mM glycine at 100 V for 2 h at 4 °C. Blots were incubated overnight at 4 °C with anti-TMEM16A antibodies (rabbit polyclonal antibodies, BA3464-2, 1:1000, BOSTER), or anti-GAPDH antibodies (rabbit polyclonal antibodies, AF0911-BP 1:5000, Affinity Biosciences) for 12 h. The membranes were then probed with the immunoreactivity by adding secondary antibody (goat anti-rabbit IgG, WLA023, 1:5000, Wanleibio) detecting it with chemiluminescent HRP detection kit.

In vitro *anticancer activity assay*

LA795 and 16HBE cells were seeded into each well of a 96-well plate and cultured for 24 h. Cells were then cultured with dimethyl sulfoxide (0.1% (*v*/*v*) DMSO as control) or ZAF (0–100 μM) for 48 h before performing the MTT (3-(4,5-dimethylthiazol-2-yl)-2,5-diphenyltetrazolium bromide) assay. Cells were incubated with 5 mg/ml MTT (20 μl) solution for 4 h. The sample absorbance was measured at 490 nm using a SpectraMAX i3 spectrophotometer. The percentage of cell viability was calculated by dividing the absorbance of the ZAF treated group with that of the control group.

LA795 cells were grown to achieve 90% confluency in 6-well plates, scraped with a sterile 200 μl tip, and washed twice with PBS. Then, the cells were incubated with each medium containing 1% fetal bovine serum and treated with ZAF at 25, 50, or 75 μM or 0.1% (*v*/*v*) DMSO (control). Finally, cells were photographed at 0, 24, 48, or 72 h under an inverted microscope at × 100 magnification. The wound-healing area was calculated using ImageJ software, and the relative scratch area was determined as the ratio of the average area in ZAF-treated cells to that in the control cells.

LA795 cells were seeded in 6-well plates and incubated overnight at 37 °C in a humidified and 5% CO_2 atmosphere. After being rinsed with PBS (pH 7.4), the cells were incubated with the 0.1% (*v*/*v*) DMSO (control), 50 μM, 100 μM ZAF for 36 h under the same conditions, respectively. Afterward, the cells of the experimental group were rinsed again with PBS and stained with calcein-AM and propidium iodide for visualization of live and dead/late apoptotic cells, respectively. Finally, the cells of all groups were rinsed again with PBS and were observed by confocal fluorescence microscopy.

Tumor xenografts in mice

All animal studies were approved by the Laboratory Animal Ethical and Welfare Committee Hebei Medical University. No statistical method was applied to predetermine the sample size, and the investigators performing preclinical experiments were not blinded. LA795 cells (5×10^6 cells per mouse) were inoculated to the right forelimb of BALB/c nude mice (about 6 weeks, male). After the tumor volume reached 50 mm^3, the mice were divided into four groups in a randomized manner: control group, cisplatin group (6.5 mg/kg), low-dose ZAF group (2.9 mg/kg), and high-dose ZAF group (5.8 mg/kg), six samples per group. Mice in the cisplatin and ZAF groups were injected with 0.1 ml of working solution every 2 days, while control group mice were injected with 0.1 ml of saline. Tumor size was measured with caliper, and volume was calculated with the standard formula: length × $width^2/2$. Weight of mice and volume of tumors were measured every 2 days, and the mice were administered intraperitoneally. On the 15th day, the tumor tissues were excised for histological analysis.

Data analysis

Graphical presentation and data analysis were performed using OriginPro Learning Edition and Microsoft Excel 2019. The data are presented as mean ± standard deviation, and the number of replicates is given in Figure legends. Statistical significance of the differences between group means was evaluated by one-way analysis of variance using Tukey's honestly significant difference test as a post hoc test; p values ≤0.05 were considered statistically significant ($^*p < 0.05$, $^{**}p < 0.01$, $^{***}p < 0.001$ and $^{****}p < 0.0001$). Discovery Studio visualizer was used to analyze noncovalent interactions between ZAF

and its binding pocket. Visualization and analysis of model features were performed by VMD (49) and Open-Source Pymol (https://pymol.org).

Data availability

The data that support the findings of this study are available from the corresponding author upon reasonable request.

Author contributions—S. S. and H. A. conceptualization; S. S. methodology; S. S. writing-original draft; B. M. data curation; B. M. formal analysis; F. S. and D. S. investigation; C. Q. validation; W. L. and H. A. project administration; G. L. software; H. Z. resources; H. A. supervision.

Funding and additional information—This work was supported by the National Natural Science Foundation of China (Grant No. 81830061 to H. A.), the Natural Science Foundation of Tianjin of China (Grant No. 19JCYBJC28300 to H. A.), the Natural Science Foundation of Hebei Province of China (Grant No. H2020202005 to H. A.), and the Tianjin Municipal Education Commission of China (Grant No. 2019ZD033 to W. L.)

Conflict of interest—The authors declare no conflict of interests.

Abbreviations—The abbreviations used are: 16HBE, human bronchial epithelial cells; Da, Dalton; FDA, Food and Drug Administration; HEK293T, human embryonic kidney 293T cells; I–V, current–voltage; LA795, lung adenocarcinoma 795 cells; MD, Molecular dynamics; ZAF, Zafirlukast.

References

1. Stewart, B., and Wild, C. (2014) *World Cancer Report 2014*, International Agency for Research on Cancer, Lyon, France
2. Ferlay, J., Colombet, M., Soerjomataram, I., Parkin, D. M., and Bray, F. (2021) Cancer statistics for the year 2020: An overview. *Int. J. Cancer* **149**, 778–789
3. Barta, J. A., Powell, C. A., and Wisnivesky, J. P. (2019) Global epidemiology of lung cancer. *Ann. Glob. Health* **85**, 8
4. Jia, L., Liu, W., Guan, L., Lu, M., and Wang, K. W. (2015) Inhibition of calcium-activated chloride channel ANO1/TMEM16A suppresses tumor growth and invasion in human lung cancer. *PLoS One* **10**, e0136584
5. Xin, H., Gollin, S. M., Raja, S., and Godfrey, T. E. (2002) High-resolution mapping of the 11q13 amplicon and identification of a gene, TAOS1, that is amplified and overexpressed in oral cancer cells. *Proc. Natl. Acad. Sci. U. S. A.* **99**, 11369–11374
6. Ji, Q., Guo, S., Wang, X., Pang, C., Zhan, Y., Chen, Y., and An, H. (2019) Recent advances in TMEM16A: Structure, function, and disease. *J. Cell Physiol.* **234**, 7856–7873
7. Guo, S., Chen, Y., Pang, C., Wang, X., Shi, S., Zhang, H., An, H., and Zhan, Y. (2019) Matrine is a novel inhibitor of the TMEM16A chloride channel with antilung adenocarcinoma effects. *J. Cell Physiol.* **234**, 8698–8708
8. Zhang, X., Li, H., Zhang, H., Liu, Y., Huo, L., Jia, Z., Xue, Y., Sun, X., and Zhang, W. (2017) Inhibition of transmembrane member 16A calcium-activated chloride channels by natural flavonoids contributes to flavonoid anticancer effects. *Br. J. Pharmacol.* **174**, 2334–2345
9. Yang, Y. D., Cho, H., Koo, J. Y., Tak, M. H., Cho, Y., Shim, W. S., Park, S. P., Lee, J., Lee, B., Kim, B. M., Raouf, R., Shin, Y. K., and Oh, U. (2008) TMEM16A confers receptor-activated calcium-dependent chloride conductance. *Nature* **455**, 1210–1215
10. Caputo, A., Caci, E., Ferrera, L., Pedemonte, N., Barsanti, C., Sondo, E., Pfeffer, U., Ravazzolo, R., Zegarra-Moran, O., and Galietta, L. J. (2008) TMEM16A, a membrane protein associated with calcium-dependent chloride channel activity. *Science* **322**, 590–594
11. Schroeder, B. C., Cheng, T., Jan, Y. N., and Jan, L. Y. (2008) Expression cloning of TMEM16A as a calcium-activated chloride channel subunit. *Cell* **134**, 1019–1029
12. Sui, Y., Sun, M., Wu, F., Yang, L., Di, W., Zhang, G., Zhong, L., Ma, Z., Zheng, J., Fang, X., and Ma, T. (2014) Inhibition of TMEM16A expression suppresses growth and invasion in human colorectal cancer cells. *PLoS One* **9**, e115443
13. Ayoub, C., Wasylyk, C., Li, Y., Thomas, E., Marisa, L., Robé, A., Roux, M., Abecassis, J., De Reyniès, A., and Wasylyk, B. (2010) ANO1 amplification and expression in HNSCC with a high propensity for future distant metastasis and its functions in HNSCC cell lines. *Br. J. Cancer* **103**, 715–726
14. Bill, A., Hall, M. L., Borawski, J., Hodgson, C., Jenkins, J., Piechon, P., Popa, O., Rothwell, C., Tranter, P., Tria, S., Wagner, T., Whitehead, L., and Gaither, L. A. (2014) Small molecule-facilitated degradation of ANO1 protein: A new targeting approach for anticancer therapeutics. *J. Biol. Chem.* **289**, 11029–11041
15. Wang, T., Wang, H., Yang, F., Gao, K., Luo, S., Bai, L., Ma, K., Liu, M., Wu, S., Wang, H., Chen, Z., and Xiao, Q. (2021) Honokiol inhibits proliferation of colorectal cancer cells by targeting anoctamin 1/TMEM16A Ca(2+) -activated Cl(-) channels. *Br. J. Pharmacol.* **178**, 4137–4154
16. Namkung, W., Phuan, P. W., and Verkman, A. S. (2011) TMEM16A inhibitors reveal TMEM16A as a minor component of calcium-activated chloride channel conductance in airway and intestinal epithelial cells. *J. Biol. Chem.* **286**, 2365–2374
17. Huang, F., Zhang, H., Wu, M., Yang, H., Kudo, M., Peters, C. J., Woodruff, P. G., Solberg, O. D., Donne, M. L., Huang, X., Sheppard, D., Fahy, J. V., Wolters, P. J., Hogan, B. L., Finkbeiner, W. E., *et al.* (2012) Calcium-activated chloride channel TMEM16A modulates mucin secretion and airway smooth muscle contraction. *Proc. Natl. Acad. Sci. U. S. A.* **109**, 16354–16359
18. Shi, S., Guo, S., Chen, Y., Sun, F., Pang, C., Ma, B., Qu, C., and An, H. (2020) Molecular mechanism of CaCCinh-A01 inhibiting TMEM16A channel. *Arch. Biochem. Biophys.* **695**, 108650
19. Shi, S., Ma, B., Sun, F., Qu, C., and An, H. (2021) Theaflavin binds to a druggable pocket of TMEM16A channel and inhibits lung adenocarcinoma cell Viability. *J. Biol. Chem.* **297**, 101016
20. Sleire, L., Førde-Tislevoll, H. E., Netland, I. A., Leiss, L., Skeie, B. S., and Enger, P. (2017) Drug repurposing in cancer. *Pharmacol. Res.* **124**, 74–91
21. Kola, I., and Landis, J. (2004) Can the pharmaceutical industry reduce attrition rates? *Nat. Rev. Drug Discov.* **3**, 711–716
22. Wang, H., Zou, L., Ma, K., Yu, J., Wu, H., Wei, M., and Xiao, Q. (2017) Cell-specific mechanisms of TMEM16A Ca2+-activated chloride channel in cancer. *Mol. Cancer* **16**, 152
23. Hay, M., Thomas, D. W., Craighead, J. L., Economides, C., and Rosenthal, J. (2014) Clinical development success rates for investigational drugs. *Nat. Biotechnol.* **32**, 40–51
24. Pan, P., Bouche, G., Meheus, L., Sukhatme, V., and Vikas, P. (2014) The repurposing drugs in oncology (ReDO) Project. *Ecancermedicalscience* **8**, 442
25. Nguyen, T., Syed, A., Ibrahim, S., Guo, J., and Bai, B. (2018) DeCoST: A new approach in drug repurposing from control system theory. *Front. Pharmacol.* **9**, 583
26. Dudley, J. T., Tarangini, D., and Butte, A. J. (2011) Exploiting drug–disease relationships for computational drug repositioning. *Brief. Bioinform.* **12**, 303–311
27. Silverman, R. A., Nowak, R. M., Korenblat, P. E., Skobeloff, E., Chen, Y., Bonuccelli, C. M., Miller, C. J., and Simonson, S. G. (2004) Zafirlukast treatment for acute asthma: Evaluation in a randomized, double-blind, multicenter trial. *Chest* **126**, 1480–1489
28. Wunder, F., Tinel, H., Kast, R., Geerts, A., Becker, E. M., Kolkhof, P., Hütter, J., Ergüden, J., and M, H. (2010) Pharmacological characterization of the first potent and selective antagonist at the cysteinyl leukotriene 2 (CysLT(2)) receptor. *Br. J. Pharmacol.* **160**, 399–409
29. Spector, S. L., Smith, L. J., and Glass, M. (1994) Effects of 6 weeks of therapy with oral doses of ICI 204,219, a leukotriene D4 receptor

antagonist, in subjects with bronchial asthma. ACCOLATE Asthma Trialists Group. *Am. J. Respir. Crit. Care Med.* **150**, 618–623
30. Krell, R. D., Aharony, D., Buckner, C. K., Keith, R. A., Kusner, E. J., Snyder, D. W., Bernstein, P. R., Matassa, V. G., Yee, Y. K., and Brown, F. J. (1990) The preclinical pharmacology of ICI 204,219. A peptide leukotriene antagonist. *Am. Rev. Respir. Dis.* **141**, 978–987
31. Göbel, T., Diehl, O., Heering, J., Merk, D., Angioni, C., Wittmann, S. K., Buscato, E. L., Kottke, R., Weizel, L., and Schader, T. (2019) Zafirlukast is a dual modulator of human soluble epoxide hydrolase and peroxisome proliferator-activated receptor γ. *Front. Pharmacol.* **10**, 263
32. Holbrook, L., Keeton, S., Sasikumar, P., Nock, S., Gelzinis, J., Brunt, E., Ryan, S., Pantos, M., Verbetsky, C., Gibbins, J., and Kennedy, D. (2021) Zafirlukast is a broad-spectrum thiol isomerase inhibitor that inhibits thrombosis without altering bleeding times. *Br. J. Pharmacol.* **178**, 550–563
33. Figueroa, E. E., Kramer, M., Strange, K., and Denton, J. S. (2019) CysLT1 receptor antagonists pranlukast and zafirlukast inhibit LRRC8-mediated volume regulated anion channels independently of the receptor. *Am. J. Physiol. Cell Physiol.* **317**, C857–C866
34. Luginina, A., Gusach, A., Marin, E., Mishin, A., and Cherezov, V. (2019) Structure-based mechanism of cysteinyl leukotriene receptor inhibition by antiasthmatic drugs. *Sci. Adv.* **5**, eaax2518
35. Guo, S., Chen, Y., Shi, S., Wang, X., Zhang, H., Zhan, Y., and An, H. (2020) Arctigenin, a novel TMEM16A inhibitor for lung adenocarcinoma therapy. *Pharmacol. Res.* **155**, 104721
36. Guo, S., Bai, X., Liu, Y., Shi, S., Wang, X., Zhan, Y., Kang, X., Chen, Y., and An, H. (2021) Inhibition of TMEM16A by natural product silibinin: Potential lead compounds for treatment of lung adenocarcinoma. *Front. Pharmacol.* **12**, 643489
37. Shi, S., Pang, C., Guo, S., Chen, Y., Ma, B., Qu, C., Ji, Q., and An, H. (2020) Recent progress in structural studies on TMEM16A channel. *Comput. Struct. Biotechnol. J.* **18**, 714–722
38. Paulino, C., Kalienkova, V., Lam, A. K. M., Neldner, Y., and Dutzler, R. (2017) Activation mechanism of the calcium-activated chloride channel TMEM16A revealed by cryo-EM. *Nature* **552**, 421–425
39. Waterhouse, A., Bertoni, M., Bienert, S., Studer, G., Tauriello, G., Gumienny, R., Heer, F. T., de Beer, T. A. P., Rempfer, C., Bordoli, L., Lepore, R., and Schwede, T. (2018) SWISS-MODEL: Homology modelling of protein structures and complexes. *Nucleic Acids Res.* **46**, W296–W303
40. Bienert, S., Waterhouse, A., de Beer, T. A. P., Tauriello, G., Studer, G., Bordoli, L., and Schwede, T. (2017) The SWISS-MODEL Repository-new features and functionality. *Nucleic Acids Res.* **45**, D313–D319
41. Trott, O., and Olson, A. J. (2010) AutoDock Vina: Improving the speed and accuracy of docking with a new scoring function, efficient optimization, and multithreading. *J. Comput. Chem.* **31**, 455–461
42. Morris, G. M., Huey, R., Lindstrom, W., Sanner, M. F., Belew, R. K., Goodsell, D. S., and Olson, A. J. (2009) AutoDock4 and AutoDockTools4: Automated docking with selective receptor flexibility. *J. Comput. Chem.* **30**, 2785
43. Brooks, B. R., Brooks, C. L., III, Mackerell, A. D., Jr., Nilsson, L., Petrella, R. J., Roux, B., Won, Y., Archontis, G., Bartels, C., and Boresch, S. (2009) CHARMM: The biomolecular simulation program. *J. Comput. Chem.* **30**, 1545
44. Case, D., Betz, R., Cerutti, D. S., Cheatham, T., Darden, T., Duke, R., Giese, T. J., Gohlke, H., Götz, A., Homeyer, N., Izadi, S., Janowski, P., Kaus, J., Kovalenko, A., Lee, T.-S., *et al.* (2016) *Amber 2016*, University of California, San Francisco
45. Li, P., and Merz, K. M. (2014) Taking into account the ion-induced dipole interaction in the nonbonded model of ions. *J. Chem. Theory Comput.* **10**, 289–297
46. Li, P., Roberts, B. P., Chakravorty, D. K., and Merz, K. M. (2013) Rational design of Particle Mesh Ewald compatible Lennard-Jones parameters for +2 metal cations in explicit solvent. *J. Chem. Theory Comput.* **9**, 2733–2748
47. Frisch, M. J., Trucks, G. W., Schlegel, H. B., Scuseria, G. E., Robb, M. A., Cheeseman, J. R., Montgomery, J. A., Jr., Vreven, T., Kudin, K. N., Burant, J. C., Millam, J. M., Iyengar, S. S., Tomasi, J., Barone, V., Mennucci, B., *et al.* (2003) *Gaussian 03*
48. Tian, L., and Feiwu, C. (2012) Multiwfn: A multifunctional wavefunction analyzer. *J. Comput. Chem.* **33**, 580–592
49. Humphrey, W., Dalke, A., and Schulten, K. (1996) VMD: Visual molecular dynamics. *J. Mol. Graph.* **14**, 33–38